

SHAFT POWER MEASUREMENTS IN A TRANSIENT TURBINE TEST FACILITY

Nicholas R. Atkins*

Department of Engineering Science
University of Oxford
Email: nicholas.atkins@eng.ox.ac.uk

Roger W. Ainsworth

Department of Engineering Science
University of Oxford

ABSTRACT

Transient test facilities offer the potential for the simultaneous study of turbine aerodynamic performance, unsteady flow phenomena and the heat transfer characteristics of a turbine stage. This paper describes the accurate measurement of the shaft power generated by the turbine in the Oxford Rotor Facility (ORF), one of the key requirements for aerodynamic performance testing.

A high resolution encoder system has been developed for the accurate measurement of the turbine speed and acceleration. The desired accuracy and frequency response specifications of the system are outlined. The method that has been developed to characterise the error signature of the encoder disc and the signal processing used to remove it are also outlined. The measurement of the losses due to disc windage and bearing friction are also described.

Introduction

The practical performance, both the efficiency and durability, of a high pressure turbine depends on many interrelated factors. These include both the steady and unsteady aerodynamics as well as the heat transfer characteristics. Continual increases in turbine inlet temperature mean that the practical limits of a new turbine design can often be lead by heat transfer considerations. Traditionally the aerodynamic performance of new turbine designs has been tested in large scale steady flow rigs, but the very high cost of such facilities means that their use is becoming limited. Transient test techniques at engine representative conditions offer a comparatively low cost alternative. The engine representative gas-to-wall temperature ratio of transient test facilities enables the study of heat transfer. Performance testing in transient facilities allows the simultaneous study of the aerodynamic performance penalties/gains associated with geometry changes motivated by heat transfer considerations.

The current ORF working section features a 62% scale, 1-1/2 stage, high-pressure shroudless transonic turbine. The required inlet flow conditions are provided by an Isentropic Light Piston Tunnel (ILPT) with a quasi-steady state run time of approximately 100ms. The testing is conducted at engine representative specific speed, pressure ratio, gas-to-wall temperature

ratio, Mach number and Reynolds number.

The measurement of turbine efficiency or aerodynamic performance requires a measure of the actual aerodynamic power produced. In any turbine test facility the power produced by the turbine must be absorbed. Steady flow test facilities operate at nominally constant speed and the power is absorbed by some form of brake. Transient test facilities fall into two basic categories, those that run at nominally constant speed through the use of a brake [1,2], and those in which the turbine disc is free to accelerate during testing, such as the ORF [3]. The mode of operation of transient test facilities presents a fundamentally different shaft power measurement problem when compared to steady flow facilities.

NOMENCLATURE

AGV Annular Gate Valve
 C_* Influence coefficient for variable *
 C Capacitance
DAQ Data acquisition
FFT Fast Fourier Transform
 I Polar moment of inertia
 l Encoder Line
 \dot{m} Mass flow rate
 n Sample
 N Number of encoder lines
NGV High pressure Nozzle Guide Vane
ORF Oxford Rotor Facility
 P Total pressure
 P_r Pressure ratio
 R Radius, resistance
RSS Root Square Sum addition
 S_{95*} 95% coverage precision limit for variable *
 t time
 T Torque, temperature
 \dot{W}_s Shaft power
 ε Eccentricity
 η Efficiency
 ω Angular speed
 Ω FFT of angular speed
 $\dot{\omega}$ Angular acceleration
 θ Angular position

*Address all correspondence to this author.

Subscripts

- 0 Total conditions
- 1 HP NGV inlet conditions
- actual* Actual value
- f* Frequency, feedback path value

Shaft Power Measurement Theory

Due to various losses, the power measured at the turbine shaft will be slightly lower than the actual aerodynamic power produced by the turbine. The net torque on the turbine shaft is the sum of the aerodynamic torque produced by the turbine blades, T_{aero} , the brake torque on the shaft, T_{brake} , the drag torque due to bearing friction, $T_{bearings}$, and the aerodynamic drag or windage on the faces of the rotor disc, $T_{windage}$. A free

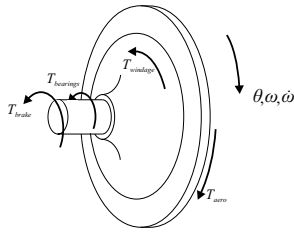


Figure 1. Free body diagram of a rotor disc

body diagram of the forces acting on the rotor disc is shown in figure 1. Considering rotational equilibrium, the equation of motion for the disc is

$$\sum T_{net} = I \frac{d^2\theta}{dt^2} = I\dot{\omega} = T_{aero} - T_{brake} - T_{windage} - T_{bearings} \quad (1)$$

This equation can be rearranged to give the aerodynamic torque produced by the turbine,

$$T_{aero} = I\dot{\omega} + T_{brake} + T_{windage} + T_{bearings} \quad (2)$$

The actual aerodynamic power produced by the turbine is then given by eq. 3 below.

$$\dot{W}_{s_{actual}} = T_{aero}\omega = (I\dot{\omega} + T_{brake} + T_{windage} + T_{bearings})\omega \quad (3)$$

In steady state test facilities the brake torque is used to absorb the power produced by the turbine and maintain a constant speed. The inertial power term, $I\dot{\omega}$, in eq. 3 approaches zero and the actual power produced can be derived from the product of the measured brake torque and the disc speed. In transient test facilities such as the ORF where the turbine is free to accelerate during testing, there is no brake torque. As such, the actual aerodynamic power can be calculated from just the measured speed, acceleration, inertia, and drag torque.

In comparison to steady flow testing, the key to accurate power measurements in a transient facility is the bandwidth of the measurement system.

Moment of inertia The inertia of the entire ORF rotating assembly has been measured by a trifilar suspension technique [4]. It was measured at 1.64 kgm² to an uncertainty of $\pm 1\%$. For a testing program in which the rotating assembly is unchanged this is a pure bias error, and has no effect on the precision uncertainty, or resolution, of the efficiency measurement. Examples include parametric studies of efficiency versus specific speed, pressure ratio, specific mass flow, or the study of a casing, or NGV geometry modification. However if any of the rotating parts are changed the precision uncertainty of the measured change in inertia will affect the precision uncertainty of the overall efficiency measurement.

Losses It will be shown in the next section that the uncertainty in the measurement of these losses is attenuated by two orders of magnitude due to their relative size in comparison to the total power produced by the turbine. This means that they only need to be measured to an uncertainty of $\pm 5\%$ in order to ensure that their influence on the overall efficiency measurement uncertainty is insignificant. The measurement of the losses is discussed at the end of this paper.

Rotational speed and acceleration During a typical test run the turbine disc accelerates from approximately 7100 rpm to 9900 rpm in 230 ms, producing a mean aerodynamic power of approximately 2.1 MW. The next section outlines the development of a high resolution encoder system to measure the speed and hence the acceleration of the turbine disc during the operation of the ORF.

Encoder System Specifications

The need to resolve changes in turbine efficiency to a precision uncertainty in the region of $\pm 0.3\%$ sets the target precision uncertainty of the actual power measurement, $S_{95_{W_s}}$, at approximately $\pm 0.2\%$. This section translates this overall uncertainty target into a more detailed specification for the encoder system.

Precision uncertainty

The analysis that follows concerns a single point measurement precision uncertainty. Attenuation of signal components corresponding to the piston oscillation will have a high degree of correlation across a set of measurements. The distribution of error is unlikely to be normal, so a single point measurement uncertainty, although a worst-case estimate, is the most suitable design target. In order to determine the target uncertainty limits, S_{95_e} , for each of the measured variables, the propagation of error through to the final measurement has been analysed.

The influence coefficients for each of the measured variables are evaluated using the standard procedure [5] and they are summarised in table 1. The total precision uncertainty is found using Root Square Sum (RSS) addition. In this situation

Table 1. Power measurement influence coefficients

Measurement	Influence Coefficient C_*	Value
C_I	$\frac{1}{1 + \frac{T_{drag}}{T\omega}}$	0.98
$C_{\dot{\omega}}$	$\frac{1}{1 + \frac{T_{drag}}{T\omega}}$	0.98
C_{ω}	1	1
$C_{T_{drag}}$	$\frac{1}{1 + \frac{T\omega}{T_{drag}}}$	0.02

the acceleration is derived from the measurement of speed by numerical differentiation. As such, the acceleration precision uncertainty is a function of both the signal processing scheme used to derive it and the uncertainty in the speed signal. The speed, and hence acceleration signals are made up of several frequency components, so the uncertainty level at any given frequency is governed by the frequency response of the system. The next section breaks down the ideal power signal into discrete frequency components in order to specify the speed measurement precision limit, $S_{95\omega}$ at the relevant frequencies.

Rotor speed measurement uncertainty

The turbine shaft power, $\dot{W}_{s_{actual}}$, can be expressed as a function of the turbine efficiency, η , pressure ratio, P_r , mass flow rate, \dot{m} , and the inlet total temperature, T_{01} .

$$\dot{W}_{s_{actual}} = \eta \cdot \dot{m} c_p T_{01} \left\{ P_r^{\frac{\gamma-1}{\gamma}} - 1 \right\} \quad (4)$$

The flow conditions are driven primarily by the stage inlet total pressure, P_{01} , which is linked to the stagnation conditions in the piston tube. The inlet nozzle guide vanes are almost choked and the stage mass flow rate is a function of the inlet total pressure and temperature only. The inlet total temperature is related to the inlet total pressure by the almost isentropic conditions in the pump tube. Neglecting the subtle changes in pressure ratio and efficiency, the actual shaft power can therefore be considered as a function of the stage inlet total pressure alone.

The stage inlet total pressure during a typical operation of the ORF is shown in figure 2. The period of operation during which the flow is on-condition, the *test window*, is shown in the lower plot. The inlet total pressure signal can be broken down into several components at specific frequencies. The starting process of the run is approximately equivalent to a 1.3 Hz pulse. The $\pm 1\%$, 25 Hz variation in total pressure is caused by the finite piston mass (the *piston oscillation*) and the smaller $\pm 0.3\%$, 250 Hz oscillation is a reflected pressure wave. As the shaft power is approximately proportional to the inlet total pressure it can be considered to consist of equivalent components.

The acceleration of the rotor disc is derived directly from the speed signal by differentiation. The ideal differentiation process has magnitude, $|G(j\omega)| = \omega$, and phase $\angle j\omega = 90^\circ$. The differentiation process amplifies uncertainty in the speed signal at a given frequency, f , by a factor $2\pi f$. Consequentially, the acceleration uncertainty will dominate the RSS addition.

The frequency response of the speed measurement system gives the attenuation of a signal at each frequency. The speed er-

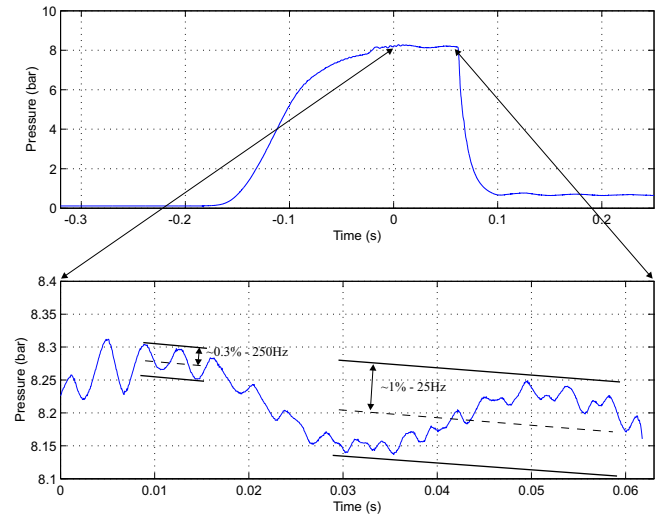


Figure 2. Typical time history of stage inlet total pressure, P_{01}

ror due to this attenuation is amplified by the differentiation process, giving rise to uncertainty in the measured power. Therefore this attenuation (or frequency response) can be considered as a contribution to the precision uncertainty at a given frequency. The overall error budget must be set by accounting for the uncertainty due to each of the components at their respective frequencies.

Error Budget For each component of the ideal power signal the contribution to the total acceleration precision uncertainty is found from the product of the speed error at that frequency, $S_{95\omega}$, the speed, ω , and the relative magnitude of the component. The components of the inlet total pressure and hence the ideal power signal are tabulated in table 2. Uncertainties in the measurement of the starting pulse of the

Table 2. Break down of the ideal power signal

Component	Frequency	Magnitude	ω	Uncertainty in $\dot{\omega}$
Starting pulse	≤ 1.3 Hz	100% of FS	$\leq 2.6\pi$ rads $^{-1}$	$8.2S_{95\omega}$ at 1.3 Hz
Piston oscill	~ 25 Hz	$\pm 1\%$ of FS	50π rads $^{-1}$	$1.6S_{95\omega}$ at 25 Hz
Pressure wave	~ 250 Hz	$\pm 0.3\%$ of FS	400π rads $^{-1}$	$2.5S_{95\omega}$ at 250 Hz

run at 1.3 Hz are amplified by a factor of 8.2, uncertainty in the measurement of the piston oscillation at 25 Hz is amplified by a factor of 1.6. Consequentially, the speed measurement requires an uncertainty of approximately an order of magnitude lower than that of the acceleration measurement to achieve the target shaft power uncertainty, $S_{95\dot{W}_s}$, of $\pm 0.2\%$. The required precision limits are summarised in table 3. The total speed measurement uncertainty, $S_{95\omega}$, of $\pm 0.02\%$ corresponds to approximately ± 1.8 rpm. The total acceleration uncertainty is given by the RRS addition of the individual contributions; each due to the attenuation of rotor speed at a particular frequency. The amplifications tabulated in table 2 are effectively the influence

Table 3. Target precision limits

Variable	C_s	S_{95_s}	$C_s S_{95_s}$
Acceleration, $\dot{\omega}$	0.98	$\pm 0.18\%$	$\pm 0.18\%$
Speed, ω	1	$\pm 0.02\%$	$\pm 0.02\%$
Parasitic drag, T_{drag}	0.02	$\pm 5\%$	$\pm 0.1\%$
RSS total $S_{95_{\dot{\omega}}}$			$\approx \pm 0.2\%$

coefficients. The speed measurement uncertainty target at each frequency is set to give the target total acceleration uncertainty of $\pm 0.18\%$. They are tabulated in table 3.

Table 4. Speed uncertainty breakdown

Component	$C_{\omega}(f)$	$S_{95_{\omega}}(f)$	$C_{\omega}(f)S_{95_{\omega}}(f)$
Starting pulse	8.2	$\pm 0.01\%$ of Full Scale	$\pm 0.08\%$
Piston oscillation	1.6	$\pm 0.1\%$ of 25 Hz component	$\pm 0.16\%$
Pressure reflection	2.5	$\pm 0.01\%$ of 200 Hz component	$\pm 0.03\%$
RSS Total $S_{95_{\omega}}$			$\approx \pm 0.18\%$

The measurement of speed from the raw encoder signal effectively averages over a number of encoder pulses, this process has inherent attenuation with increasing frequency. As such the 250 Hz speed uncertainty target is un-realistic, and the signal must be bandlimited below this frequency.

Summary of the encoder specifications The encoder system target specifications are summarised below:

- Overall rotor speed precision uncertainty - $S_{95_{\omega}} \approx \pm 0.02\%$
 - $S_{95_{\omega}} \approx \pm 0.01\%$, for components at **1.3 Hz**
 - $S_{95_{\omega}} \approx \pm 0.1\%$, for components at **25 Hz**
- Overall rotor acceleration precision uncertainty - $S_{95_{\dot{\omega}}} \approx \pm 0.18\%$
- Drag torque precision uncertainty $S_{95_{T_{drag}}} \approx \pm 5\%$

The basic parameters for the design of the encoder system are the type of pickup, the number of circumferential lines or marks on the disc, and the signal processing scheme. In order to achieve these uncertainty limits, the frequency response of various prototype signal processing schemes has been investigated, the results are discussed in the following section.

Prototype Signal Processing Design

The raw encoder signal has the form of a square wave. The encoder signal can be considered as a frequency modulated signal where the instantaneous frequency encodes the instantaneous speed. The carrier frequency of the encoder signal can be considered as the product of the nominal rotational speed (in Hz) and the number of lines on the encoder, N_{disc} . Higher frequency components of the speed signal, such as the linear rise and the piston oscillation, effectively modulate the frequency of the underlying carrier. The rotational speed of the disc, ω , is the time differential of the angular position, θ . The choice of numerical differentiation scheme determines the frequency response and noise sensitivity of the speed measurement.

Revolution average technique

A real encoder signal has two basic sources of uncertainty [6]. Noise in the signal corrupts the position and hence timing of the individual edge crossings, giving a differential error. Errors in the position of the encoder lines or marks, leads to an integral error in the speed signal, which rotates with the disc. This erroneous signal is known as the *disc characteristic*. The traditional way to remove the disc characteristic is to average the speed over a complete revolution of the disc. This completely removes the integral error due to errors in the position of the encoder marks.

Frequency response A MATLAB® numerical model was used to establish the frequency response of the revolution average technique at a series of discrete frequencies. It has a gain of zero at integer multiples of the normalised frequency, but more importantly it has progressive roll off from dc upwards. It has an attenuation of approximately 5% at the piston oscillation frequency of 25 Hz. This is significantly more than the target specifications for the ORF speed measurement system. The analysis suggests that the revolution average technique has insufficient bandwidth for accurate power measurements in transient facilities in general.

Fractional revolution average

To improve the frequency response of the speed measurement, the numerical differentiation scheme needs to average the speed over a smaller fraction of the disc. However, this not only means that the integral error of the disc characteristic must be removed by signal processing, but the shorter the time period over which the speed is averaged, the higher the sensitivity of the measurement to noise. The largest fractional average that satisfies the 25 Hz frequency response specification represents a moving average computed over $1/7^{th}$ of the disc. In practice time-domain based speed measurement is computationally quite efficient, but it is extremely sensitive to noise. Each individual speed sample is effectively based on only two bits of information, or samples. Quantisation and system noise as well as imperfections in the encoder marks corrupt the measured position of the line edges, and the differentiation process amplifies these errors. A section of the measured disc speed from a real encoder is shown in figure 3. The blue line shows the disc speed as calculated using a $1/6^{th}$ of a revolution average scheme. It is clearly corrupted by noise, and even with careful outline rejection and digital filtering the measurement is unlikely to meet the required specifications. The red line shows the results of a frequency domain based measurement derived from the same raw encoder signal. The signal is not filtered other than by the frequency measurement technique itself. The system used to generate the signal has slightly superior frequency response to the time-domain measurement, but is almost insensitive to noise. The instantaneous speed is calculated by windowing the encoder signal and measuring the average instantaneous frequency using a Fast Fourier Transform (FFT) algorithm. This technique is commonly known as a Short-Time Fourier Transform (STFT). The technique has several advantages over the time-domain based measurement. By measuring the frequency of the encoder sig-

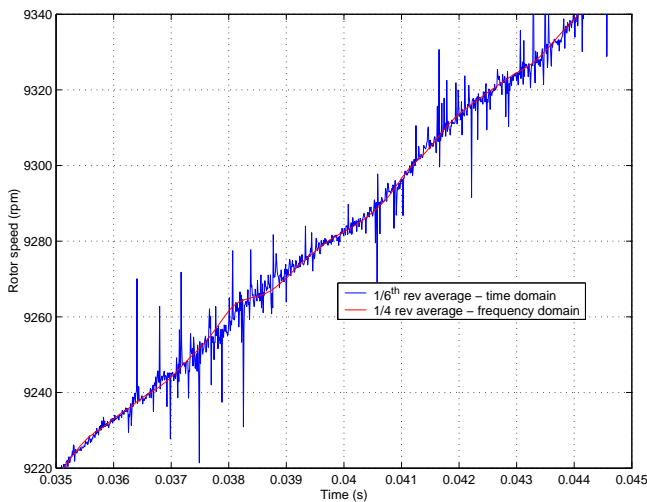


Figure 3. FFT and revolution average - detailed comparison

nal directly, a differentiation process is avoided. Each individual speed measurement is based on every sample within the windowed encoder signal, several orders of magnitude more than the time-domain based measurement. The system and quantisation noise are effectively orthogonal to the speed information. Also the effective sample rate is not limited by the number of lines on the disc, the frequency sampling window can be swept along the encoder signal, sample by sample.

These advantages are gained at the expense of the computational time required to process the encoder signals, which is several orders of magnitude longer than the time based method. The next section describes the implementation of the time-frequency transform technique for accurate speed measurements in the ORF.

STFT Speed Measurement

There are two basic design choices for the STFT signal processing system. The first is the length and type of window, which is analogous to the length of encoder over which the signal is averaged in the time-domain measurement. This choice determines the frequency response of the system. The second is the length of the FFT used, which determines the absolute resolution of the speed measurement.

The Gabor Transform

The Gabor transform is the short-time Fourier Transform with optimal time frequency resolution [7]. The windowing function is a Gaussian pulse. A unique property of a Gaussian pulse is that its frequency domain transform is also a Gaussian pulse. This property gives the Gabor Transform optimal localisation in both the time and frequency domains. The discrete version of the transform is implemented using an FFT algorithm and a truncated sampled Gaussian window. The windowing function is swept along the signal giving sections of data localised in time. The mean frequency of each section of data, (and hence disc speed) is then measured from the peaks in the instantaneous spectrum.

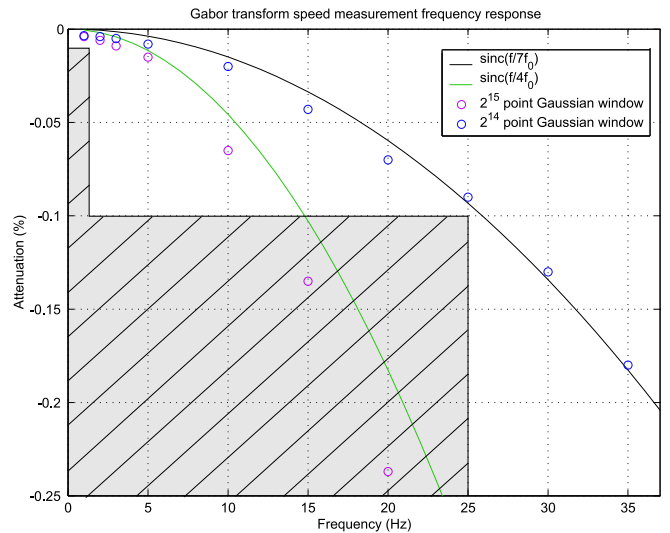


Figure 4. Effect of window length on frequency response

Frequency response testing The frequency response has been tested using the numerical model described above. The results for two different length windows are shown in figure 4. The target specifications are indicated by the shaded grey area. The Gaussian windowed measurements have increased localisation in time when compared to the time-domain revolution average. At a sample rate of 10 MHz the 2^{15} point window has a length approximately equivalent to a $1/2$ revolution average, and the 2^{14} point window has a length approximately equal to a $1/4$ of a revolution average. However, the 2^{15} and 2^{14} point Gaussian windows achieve a frequency response roughly equivalent to revolution averages of $1/4$ and $1/7$ respectively, which are shown as solid lines for comparison. The target frequency response is achieved with a 2^{14} window.

Quantization error The FFT algorithm discretises the frequency spectrum into finite sections or bins. The length of the FFT determines the width of the bins and hence the resolution of the frequency measurement. This finite resolution leads to quantization error in the measured speed signal (equivalent to the problem found in normal digital to analogue conversion). A 2^{23} point FFT is equivalent to 16 bit resolution of the fundamental of the encoder signal. Calculating the speed from the frequency of the higher harmonics increases the resolution of the measurement without increase in computation cost.

Choice of encoder line number, N_{disc} The frequency response of both time and frequency domain speed measurement techniques is determined by the fraction of the disc, and hence the length of the time window over which the speed is averaged; it is effectively independent of the number of lines on the disc. However, the number of lines on the disc determines the accuracy of the frequency measurement possible within the given window of time.

For a target resolution of disc speed, S_{ω} , at a given nominal speed, ω_0 , with an N_{disc} line encoder, the required frequency

resolution in Hz, Δf , is

$$\Delta f = \frac{\omega_0}{2\pi} N_{disc} S_\omega \quad (5)$$

The higher the number of lines on the disc, the larger the change in frequency corresponding to a given uncertainty. The Heisenberg uncertainty principal, [8]

$$\Delta t \Delta f \geq \frac{1}{4\pi} \quad (6)$$

sets the the minimum time required for a given resolution of frequency, Δf . The maximum window length, Δt , is set by the maximum fraction of the disc over which the speed can be averaged for a given frequency response target. The target uncertainty of $\pm 0.1\%$ at 25 Hz implies a minimum of 320 lines. However, the more lines, the greater the frequency resolution. Practical limits such as amplifier design, DAQ hardware, and the need for an integer multiple of the 60 rotor blades, have influenced the choice of a 660 line encoder disc.

Summary

Analysis of the target system specifications and prototype signal processing schemes have been used to set the design parameters for the encoder system. A 660 line rotary encoder disc, processed using a discrete implementation of a Gabor transform, with a 2^{23} point FFT, and a 2^{14} sample long Gaussian window have been developed.

Encoder System Design

A rotary encoder consists of a ring of marks or lines that encode the circumferential position of the disc, and a pickup system to detect the position of the marks or lines. The key factors in the design of the encoder system are:

- The position accuracy of the encoder lines
- Sensitivity of the system to noise and vibration
- Pickup system

Encoder mark position accuracy Both radial and circumferential errors in the position of the encoder lines contribute to the disc characteristic, and lead to errors in the measured rotational speed of the disc. The error in the placement of the encoder relative to the center of rotation means that the mean effective radius of the lines varies sinusoidally as the disc rotates. This eccentricity gives rise to the fundamental of the disc characteristic. Local warping of the disc and random errors in the position of the individual marks will give rise to higher harmonics in the characteristic. For an eccentricity of ϵ , and a mean encoder radius R , the error in the measured speed, $\Delta\omega$, is

$$\Delta\omega = \frac{\epsilon}{R} \sin(\omega_{disc} t) \text{ rads}^{-1} \quad (7)$$

The resultant error in the measured acceleration, $\Delta\dot{\omega}$, is found by differentiating the speed error signal

$$\Delta\dot{\omega} = \frac{\epsilon}{R_{disc}} \omega_0 \sin(\omega_0 t) \text{ rads}^{-2} \quad (8)$$

Therefore, in order to minimise the magnitude of the disc characteristic, and the resultant acceleration error, the encoder disc must be fitted at the maximum possible radius. However, the rotational speed of the rotor disc generates very high centripetal accelerations, ($\sim 32000g$ at the rotor tip), which are directly proportional to the radius. An optical encoder, which adds the lowest possible mass, and minimises the additional stresses placed of the rotor disc, has been used ¹.

Sensitivity to noise and vibration For a given level of noise, ΔV , in the encoder signal, the faster the rise time of the edges, the smaller the perturbation in the measured position of the edge, Δt . Focussing optics have been used to give a minimum spot diameter in the region of $25 \mu\text{m}$, the encoder signal has typical 10-90% rise times in the region of 700 ns.

Errors due to vibrations in the plane of rotation, such as precession of the disc about the true center of rotation are effectively random, so they cannot be removed from the encoder signal analytically. The speed of the disc is measured using two independent pickup systems mounted 180° apart to compensate for movement of the disc relative to the pickup systems.

Laser/Photodiode Pickup System The two pickup systems (one of which is shown in figure 5) consist of a rigid mounting block, a focussed diode laser, and a high speed photodiode detector. To achieve sufficient system bandwidth, high-specification low capacitance, fast response, silicon photodiodes have been used. The output of the photodiode is very low, approximately $20\mu\text{A}$, and without suitable amplification the junction capacitance of the photodiode would severely limit the bandwidth of the pickup system.

Wideband Photodiode Amplifier Design

The 660 line encoder disc, rotating at the maximum speed of 10,000rpm generates a square wave with a maximum fundamental of 110 kHz. To resolve the first 10 harmonics a bandwidth in excess of 2 MHz is required.

Current to voltage converter theory

The wideband transimpedance amplifiers are based on a very high gain-bandwidth product operational amplifier. Although the basic circuit is quite simple, the high 2 MHz bandwidth means that careful board design and phase compensation are required. At low frequencies the high open loop gain of the real op-amp means that the output voltage matches that of the

¹It would have been technically feasible to mount an encoder on a separate disc coupled to the rotor shaft, but the added complexity was unlikely to yield any significant advantages over an optical system.

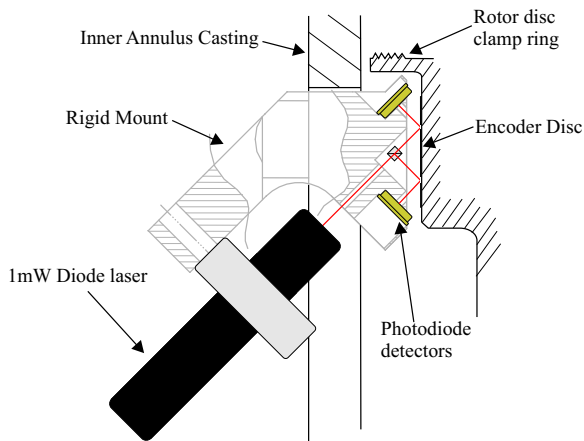


Figure 5. Schematic of the laser and photodiode pickup

ideal case. At higher frequencies, two basic factors lead to circuit instability and oscillation. Firstly the combination of the diode junction capacitance and the parasitic input capacitance of the op-amp work together with the feedback resistor R_f , to form a low pass filter in the feedback path of the circuit. This capacitance at the non-inverting input of the amplifier acts as a differentiator which leads to an increasing noise gain with frequency. Secondly the finite open loop gain of a real op-amp has first order roll-off, reaching unity gain at the gain-bandwidth product. At high frequencies the low pass filter in the feedback path gives 90° of phase lead, and the first order roll-off of the op-amps open loop gain gives 90° of phase lag. This results in an overall phase lag of 180° at high frequency, leading to potential oscillations [9]. A compensation capacitor, C_f , is chosen to provide a phase margin at high frequencies which prevents oscillation, while maximising the bandwidth of the circuit.

Data Acquisition The amplifier outputs are sampled using a National Instruments NI-5112-PXI high speed digitizer card at 20 MHz with 8 bit resolution. The digitizer has a sample timing accuracy of 2 ns seconds. The connection between the output of the amplifiers and the data-acquisition is implemented using 50Ω matched transmission lines to reduce the effects of load impedance on the output of the amplifier.

Encoder System Manufacture

The encoder disc was designed using AUTOCAD software and printed onto dimensionally stable transparent Mylar film. The printed disc is not self supporting and considerable effort was taken to mount the encoder as concentric to the center of the shaft as possible. The results of the signal processing show that the level of eccentricity of the mounted encoder disc is in the region of 0.03 mm. The next section outlines the actual signal processing used to measure the speed and acceleration of the rotor disc.



Figure 6. Detail of the printed encoder

Signal Processing

A spectrogram of a complete encoder signal from a typical test run is shown in figure 7. The horizontal axis shows increasing time, the vertical axis shows frequency, and the color shows the magnitude at a given point in the time frequency domain. Odd harmonics of the square wave signal can be distinguished up to a frequency of about 2.4 MHz. At higher frequencies the magnitude of the expected harmonics are within the noise floor. The fundamental can be seen rising from 70 to 100 kHz, together with harmonics at odd multiples. Due to the FFT resolu-

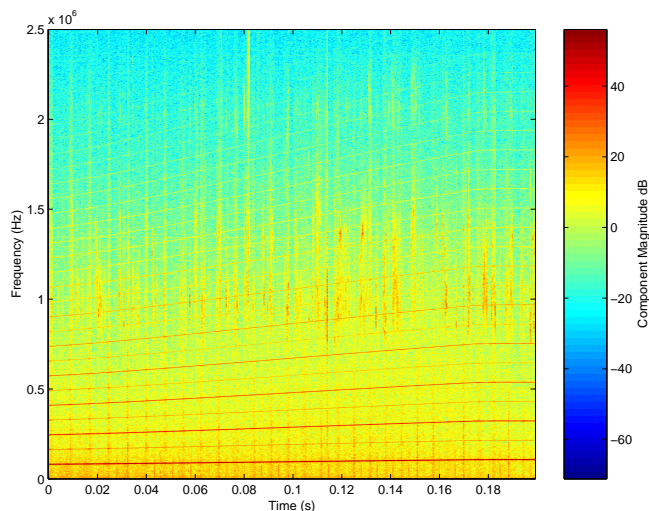


Figure 7. Spectrogram of a typical encoder signal

tion required, the processing of the encoder signals from a single run takes several hours and requires approximately 1.5GB of computer memory. The processing routine was written in MATLAB®, compiled as a stand-alone executable file, and run on the Oxford University OSWALD computing cluster.

Figure 8 shows the intermediate stages of the processing routine. Figure 8 a) shows the complete 200 ms encoder signal

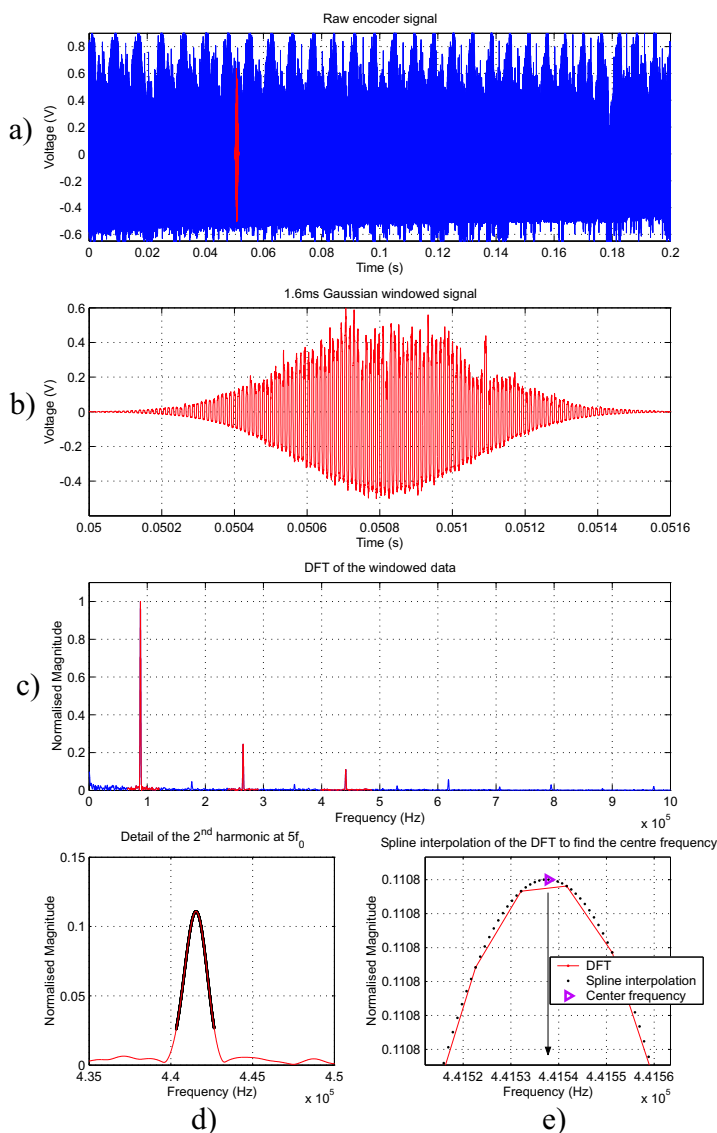


Figure 8. Detail of the Gabor Transform speed measurement

from a typical test run. The individual revolutions can be distinguished from the envelope of the signal. The characteristic envelop is due to the varied amount of light which is reflected back to the photodiode by the changing surface of the clamp ring beneath the transparent sections of the encoder. The short section of windowed data, highlighted red in figure 8 a), is shown in detail in figure 8 b). Figure 8 c) shows the computed frequency spectrum of the windowed section of data. The fundamental and the first two harmonics are shown highlighted in red. A spline fit is used to further increase the finite resolution of the FFT. Figure 8 d) shows detail of the second harmonic. The average frequency corresponds to the maximum value of the spline fit on each of the frequency peaks, as shown in Figure 8 e), and the average speed in rps is calculated from the average frequency divided by the number of lines on the disc. The Gaussian window is stepped along the encoder signal to give a sampling frequency of 20 kHz. The next section outlines the procedure for removing the disc characteristic from the processed encoder signals.

Removal of the disc characteristic

The minimum frequency of the disc characteristic (the rotational frequency of the disc) is approximately 5 times the piston oscillation frequency, however, small vibrations of the rotor disc occur close to the rotational frequency so it is desirable to remove the disc characteristic before further processing, rather than simply low pass filtering it before differentiating the speed signal.

The disc characteristic, is an error signal that rotates with the encoder disc, the fundamental is due to the eccentricity of the disc, and the higher harmonics are due to local warping and errors in the exact placement of individual lines. The harmonics of the disc characteristic are at exact integer multiples of the rotational frequency of the disc. The processed speed is a time-domain signal; a series of samples of the rotor speed at even increments of time. As the rotor accelerates, the spectrum of the disc characteristic within the time-domain speed signal is smeared out. To remove the characteristic, the time-domain speed signal is first resampled at each line passing. This gives a signal with a series of samples at even angular increments, which will be called the line-domain. Once into the line-domain the disc characteristic has a deterministic spectrum regardless of the actual speed of the rotor disc. The process of removing the characteristic is outlined below.

Edge detection An edge detection routine is used to find the exact times at which line edges pass the pickup. For accurate characterisation of the disc, the edge detection routine is designed to reject glitches.

Spline interpolation Once the line passing times have been found, the processed time-domain speed signal, $\omega(n)$, is resampled, using spline interpolation, to transform it into the line-domain signal.

Disc characteristic Eleven revolutions of high pass filtered speed signal, each 660 line-domain samples long, are shown in figure 9. The disc characteristic (indicated by the blue dots) is found from the ensemble average of the revolutions. As the disc characteristic is completely deterministic in the line-domain it is unaffected by the ensemble average. However, the real aerodynamic signal underlying the characteristic is effectively random in the line-domain, so the residual signal is attenuated by the ensemble average. This leaves an error of only ± 0.3 rpm in approximately 9000 rpm after the ensemble averaging process.

The magnitude spectrum of the line-domain disc characteristic is shown superimposed over the spectrum of a single line-domain speed signal in figure 10. The deterministic disc characteristic (blue line) is concentrated at integer multiples of the the revolution frequency, with no spectral content at all below the revolution frequency of the disc, ω_{disc} . For clarity, the speed signal has been high-pass filtered at 40 Hz to prevent the spectral leakage of the overall run shape from obscuring the signal component which can be seen at two thirds of the revolution frequency. This component is caused by small vibrations of the

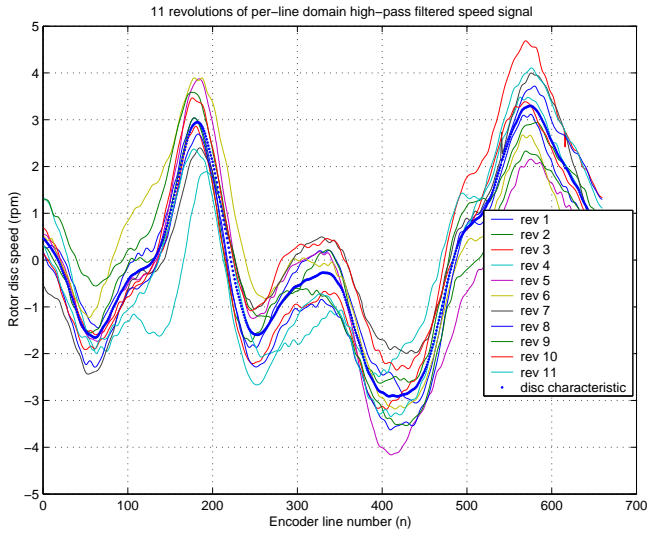


Figure 9. Eleven revolutions of line-domain speed signal

rotor disc about the true center of rotation. The magnitude of the

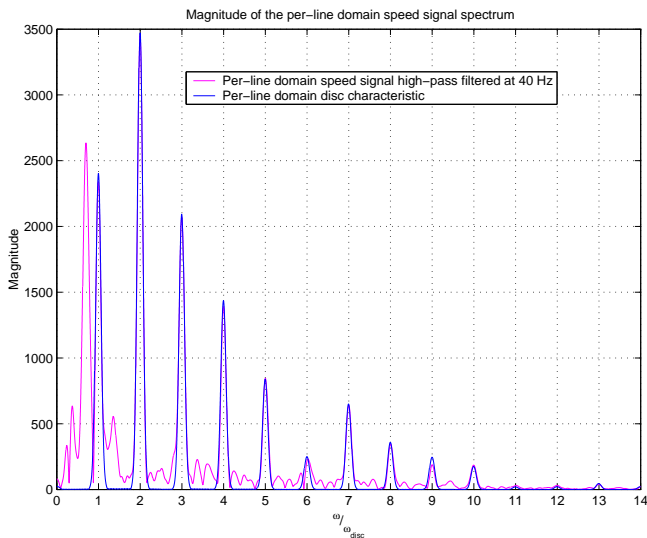


Figure 10. Magnitude spectrum of the line-domain speed signal and disc characteristic

disc characteristic fundamental suggests that the eccentricity of the printed encoder disc is in the region of 0.03 mm.

Removal of the characteristic To remove the disc characteristic, the line-domain FFT of the disc characteristic signal is subtracted from the line-domain FFT of the raw speed signal, which leaves the FFT of the line-domain corrected speed signal.

$$\Omega_{corr}(k) = FFT\{\omega_{raw}(l)\} - FFT\{\omega_{char}(l)\} \quad (9)$$

The inverse FFT of equation 9 gives the line-domain corrected speed signal.

$$\omega_{corr}(l) = IFFT\{\Omega_{corr}(k)\} \quad (10)$$

The corrected line-domain signal, $\omega_{corr}(l)$, is then transformed back to the time-domain, to give the corrected time-domain speed signal, $\omega_{corr}(n)$, by spline interpolation. The FFT processes are executed using the MATLAB® Fast Fourier Transform algorithms `fft` and `ifft`.

Acceleration The acceleration of the disc is derived from the speed measurement by numerical differentiation. Numerical approximation using a central difference Taylor series expansion gives a maximally linear digital differentiator [10]. Compared to other methods, a maximally linear response differentiator gives accurate low frequency behavior at the expense of higher frequency attenuation, extending down to a gain of 0 at the Nyquist frequency. This makes them ideal for the differentiation of the speed signals. A 5th order approximation gives negligible error at the maximum frequency of interest and has the desirable characteristic of increasing attenuation of components above 1 kHz.

Results

Rotor speed Corrected speed signals from the two pickup systems are shown in figure 11. Figure 12 shows the same signals, but high-pass filtered to highlight the high frequency detail. They are plotted in the line-domain to demonstrate the absence of the disc characteristic in the corrected speed signals; the start of each revolution is shown by a blue square. The magenta line (ω_2) shows some high frequency noise in the region of the 1 kHz which is likely to be caused by vibration of the the pickup system. Its effect on the accuracy of the measurement is negligible.

The two speed signals from the opposite pickups begin to oscillate in anti-phase at the point labeled a. This point coincides with the annular gate valve damper release, and the final onset of the flow through the turbine. The oscillation has an amplitude of between $\pm 1-2$ rpm and a frequency of about two thirds of the revolution frequency. Higher frequency components with amplitude ± 0.2 rpm at between 3 and 5 multiples of the revolution frequency can also be seen. As the measured oscillation is in anti-phase on opposite sides of the rotor disc, it must be caused by movement of the rotor disc relative to the center of rotation, and hence the encoder pickups. The motion is characteristic of a subsynchronous whirling of the rotor shaft. The whirl could be triggered by the onset of the full flow conditions, or a gyroscopic reaction to the impulse loading of the the working section when the annular gate valve dampers are released.

The subsynchronous whirl or instability is a self excited motion, often found in turbomachinery, typically at 0.3-0.8 of the shaft rotational frequency [11]. The center of the rotor disc has a complex orbit about the true center of rotation. Unlike syn-

chronous whirling it is unrelated to the imbalance of the rotor disc. It has various hypothesized causes including “oil whip” in hydrodynamic bearings, internal friction in rotating parts, and aerodynamic forces due to blade tip clearance eccentricity [11]. The oscillation has an amplitude of 2 rpm in 9000, and is measured at a radius of 207 mm, which implies a maximum deviation of ± 0.04 mm from the true center of rotation. This corresponds to approximately 5% of the rotor tip clearance. The rotational speed used to derive the acceleration is calculated from the mean of the two signals. This reduces the error to within ± 0.5 rpm, or approximately $\pm 0.006\%$ of the full scale signal. The noise and quantisation error are below this level.

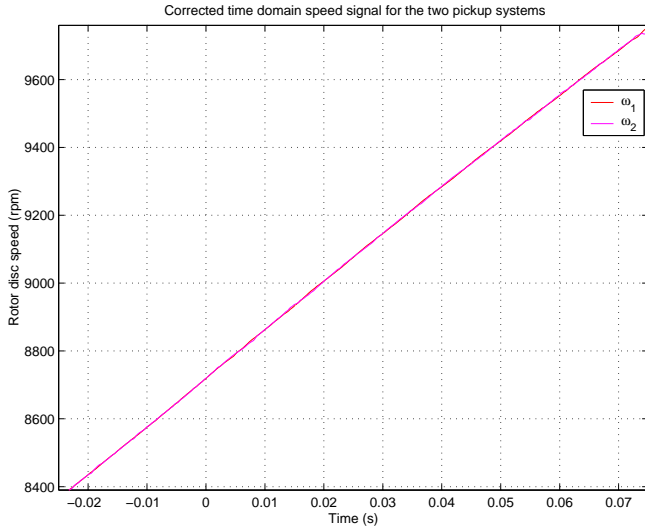


Figure 11. Corrected time-domain speed signals

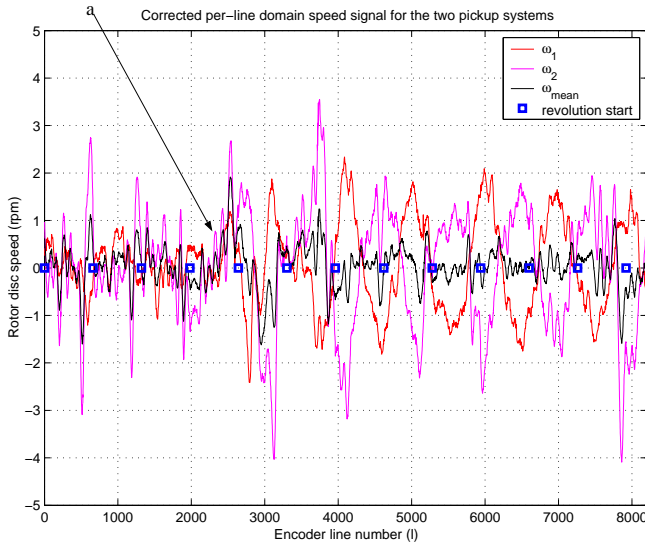


Figure 12. Corrected line-domain speed signals - high pass filtered

Turbine shaft power Once the speed signal has been numerically differentiated, the actual shaft power is calculated using eq. 3. The resulting power signal for a typical run is plotted in figure 13. The left vertical axis shows the shaft power, \dot{W}_{actual} , in Watts. The right vertical axis shows the corresponding inlet total pressure, P_{01} , in bar. The power signal can be seen to track the inlet total pressure, confirming the predictions. Compared to the pressure signal, the power signal shows an underlying rising trend. This corresponds to the changing efficiency of the turbine stage with changing rotor incidence.

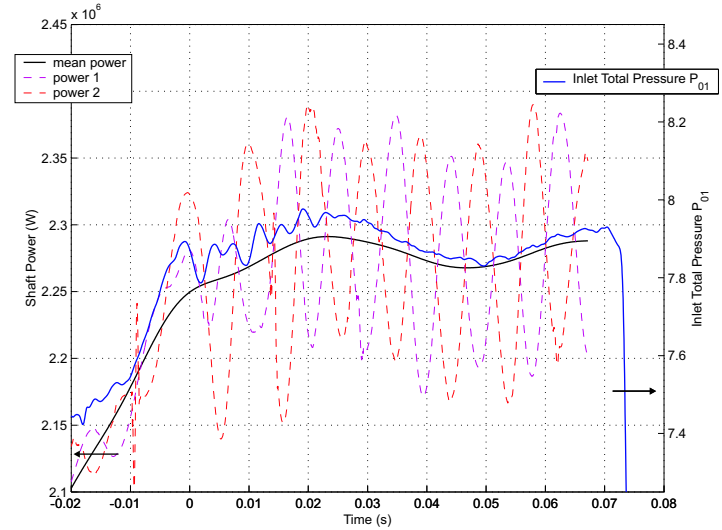


Figure 13. Actual shaft power, \dot{W}_{actual} , with inlet total pressure P_{01}

The red and magenta dotted lines show the shaft power as calculated from the individual encoder signals, the increase in the amplitude of the rotor disc vibration can be clearly seen at $t \approx -0.01$ s.

Windage and Bearing Losses

The aerodynamic torque on the faces of the rotor disc (disc windage) is approximately proportional to the square of the disc speed and the density of the the gas within the working section. The torque due to bearing friction is approximately proportional to the disc speed. Defining the following drag coefficients; static bearing friction, C_{f_0} , dynamic bearing friction, C_{f_ω} , and a windage coefficient $C_{windage}$, the power losses can be approximated using the following model.

$$P_{drag} = T_{drag}\omega = \left[C_{f_0} + C_{f_\omega}\omega + C_{windage}\frac{1}{2}\rho\omega^2 \right] \omega \quad (11)$$

A series of spin down tests have been used to establish a correlation for these power losses. During a spin down test the rotor disc is spun up using an air motor and then allowed to free-wheel to rest, the only forces acting on the rotor disc are due to bearing drag and aerodynamic windage. The deceleration of the

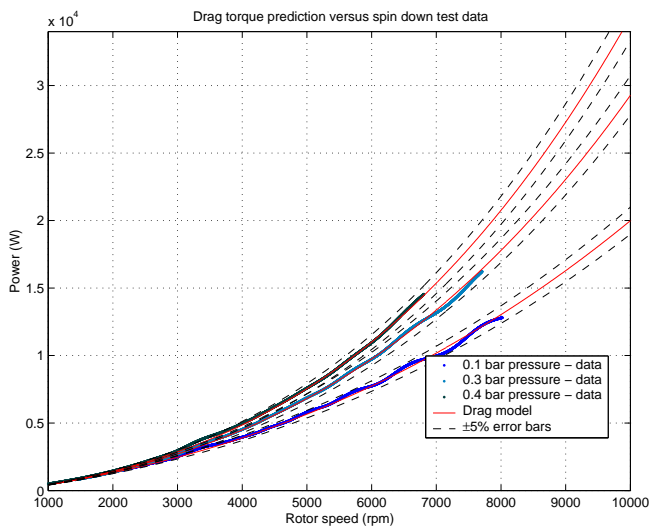


Figure 14. Drag torque prediction versus spin down test data

rotor disc is used to calculate the total drag power². The results of spin down tests at three different working section pressures are shown in figure 14. The predicted losses at the three pressures are shown by the red lines. The measured data shows good agreement with the correlation and lies within the required error bars of $\pm 5\%$, which are shown by the dashed black lines. During the on-condition test window, the average pressure within the disc cavity is proximately 0.2 bar and the rotor speed varies between approximately 8600 and 9500 rpm. The correlation predicts total power losses during the test window in the range 18-22 kW.

Conclusions

A high resolution encoder system has been developed for the measurement of turbine shaft power in a transient test facility. The encoder, pickup system, and signal processing scheme have been designed to achieve a target precision uncertainty of $\pm 0.2\%$. The encoder system achieves high fidelity speed measurements with resolution of the order 0.5 rpm in 9000, using a robust frequency domain measurement technique. A correlation has been established for the prediction of power losses during operation of the facility.

ACKNOWLEDGMENT

The authors would like to acknowledge the generous financial support provided by Rolls-Royce PLC and the UK Government Department of Trade and Industry. The authors would also like to thank Kevin Grindrod for his technical support in the operation of the facility.

²During the spin down tests the rotor blades are wind-milling and the contribution of the rotor blades to the total windage drag cannot be separated from that of the disc faces alone. The windage of the rotor blades themselves is not a parasitic error, and the spin down tests over predict the value of the disc windage.

REFERENCES

- [1] A. H. Epstein, G. R. Guenete, and R. J. G. Norton. 1984. The MIT blowdown turbine facility, ASME Paper 84-GT-116.
- [2] M. A. Hilditch, A. Fowler, T. V. Jones, K. S. Chana, M. L. G. Oldfield, R. W. Ainsworth, S. I. Hogg, S. J. Anderson, and G. C. Smith. 1994. Installation of a turbine stage in the Pyestock Isentropic Light Piston Light Piston Facility, ASME paper 94-GT-494.
- [3] R. W. Ainsworth, D. L. Schultz, M. R. D. Davies, C. J. P. Forth, M. A. Hilditch, M. L. G. Oldfield, and A. G. Sheard. *A Transient Flow Facility for the Study of the Thermofluid-Dynamics of a Full Stage Turbine Under Engine Representative Conditions*. In *Proc. of ASME Gas Turbine and Aeroengine Congress*, Amsterdam, The Netherlands, June 6-9 1988. ASME Paper 88-GT-144.
- [4] A. G. Sheard. *Aerodynamic and Mechanical Performance of a High Pressure Turbine Stage in a Transient Wind Tunnel*. D.Phil Thesis, University of Oxford, 1989.
- [5] R. B. Abernethy, R. P. Benedict and R. B. Dowdell. *ASME Measurement Uncertainty*. In *Transactions of the ASME Journal of Fluids Engineering*, volume 107, pages 161–164, June 1985.
- [6] Richard C. Kavanagh. Shaft encoder characterisation via theoretical model of differentiator with both differential and integral nonlinearities. *IEEE Transactions on Instrumentation and Measurement*, Vol. 49(No. 4):795–801, August 2000.
- [7] R. L. Allen and D. W. Mills. *Signal Analysis Time, Frequency, Scale, and Structure*. IEEE Press, Wiley Interscience, 2004.
- [8] Boualem Boashash. *Time Frequency Signal Analysis and Processing - A Comprehensive Reference*. Elsevier, 2003.
- [9] Jerald Graeme. *Photodiode Amplifiers - Op Amp Solutions*. McGraw-Hill, 1996.
- [10] C. F. Gerald and P. O. Wheatley. *Applied Numerical Analysis*. Addison-Wesley, 4th edition, 1989.
- [11] John M. Vance. *Rotordynamics of Turbomachinery*. Wiley-Interscience, 1988.